Heliyon 8 (2022) e09053

Contents lists available at ScienceDirect

Heliyon

journal homepage: www.cell.com/heliyon

Research article

A generalized numerical framework for solving cocurrent and counter-current membrane models for gas separation

Bijan Medi *, Masoud Vesali-Naseh, Mohaddeseh Haddad-Hamedani

Department of Chemical Engineering, Hamedan University of Technology, P.O. Box 65155-579, Hamedan, Iran

ARTICLE INFO

Keywords:
Gas separation
Hollow fiber membrane
Numerical method
Gauss-Seidel

ABSTRACT

Membrane separation has become a panacea for various scientific and engineering problems, including water treatment, gas separation, purification, hemodialysis, and drug delivery. Modeling and simulation of such systems are necessary for the design, analysis, and optimization of membrane separation processes. Despite numerous studies, an efficient numerical solution of such systems is an open problem, especially when speed and reliability matter. In this study, a generalized numerical framework for solving cocurrent and counter-current membrane models is proposed, which hinges on a straightforward and reliable Gauss-Seidel method with successive over-relaxation. The results confirm the speed and reliability of the proposed algorithm, while it is validated by the experimental data for the separation of a mixture of CH_4 and CO_2, as well as a mixture of He, CO_2, N_2, and CH_4. The permeate outlet pressure estimation error can be reduced to any value as low as $\sim 10^{-14}$%, while the computational time on a personal laptop is not more than 4.5 s. This algorithm can be readily implemented in various programming languages and commercial software applications.

1. Introduction

Separation processes have gained critical attention in several important fields of science and engineering. In the oil and gas industries, membrane separation plays a crucial role in CO_2 removal from sour natural gas [1] and the recovery of hydrogen and helium [2, 3, 4]. In air separation, it is used for nitrogen production [5]. It is also used for biogas purification [6] as well as in the water/wastewater treatment [7, 8, 9], food [10], and pharmaceutical industries [11]. Compared to the typical separation techniques, including cryogenic distillation, absorption, and adsorption methods, membrane technology shows higher simplicity, lower cost, moderate operating conditions, and favorable environmental features [12, 13].

Among the various membrane systems, hollow fiber membrane (HFM) modules are widely used in the separation processes because of their high interfacial area, small size, high performance, and ease of fabrication [2, 14]. HFMs consist of a large number of tubular fibers which are compactly placed in a cylindrical shell. The fibers are polymeric, inorganic-based, or mixed matrices with different lengths, internal diameters, and thicknesses in the ranges of 0.15–2 m, 63–389 μm, and 32.5–173 μm, respectively [14, 15, 16]. The performance of the membrane modules is a function of flow patterns, fiber properties, fiber configuration and operating conditions [6, 16].

In HFMs, The flow pattern can be classified into parallel flow (cocurrent and counter-current) and radial flow (cross flow). A large number of HFMs can be bundled in a shell and tube-like structure. The feed/permeate can flow either through shell or tube side [3, 17]. The design variables include feed-permeate relative direction, feed/permeate pressure, active fiber length, fiber diameter, and number of fibers [18]. The feed pressure, which provides the driving force, has been reported in the range of 4.2–80 bar for different membrane modules [16, 19]. The permeate pressure is usually close to atmospheric or relative vacuum down to 0.3 bar [20, 21]. Most of the researches have been carried out at room temperature since the increase in temperature causes a decrease in competitive gas transport through the membranes [2].

Stage-cut is defined as the ratio of permeate to feed flow and varies in the range of 0.01–0.87 by changing the feed flow rate for a constant-length membrane [3, 6].

Many attempts have been employed over the past years to evaluate the membrane processes and predict their performance in different conditions. The various numerical methods such as finite difference [22], finite element [11], shooting method [23], linear approximations [24], orthogonal collocation [5], and Runge-Kutta integration [3] have been

* Corresponding author.
E-mail address: medi@hut.ac.ir (B. Medi).

https://doi.org/10.1016/j.heliyon.2022.e09053
Received 2 November 2021; Received in revised form 9 January 2022; Accepted 1 March 2022

utilized for the solution of HFMs. But, simulating HFMs is still an open challenge due to problem complexity and also new applications that arise as technology advances. This includes flowsheeting applications in which different separation processes must be integrated and simulated seamlessly and efficiently in terms of accuracy and speed.

Hosseini et al. [25]covered the depth of modeling details for binary gas mixtures. They developed a simplified model with the assumption of ideal conditions to give a quick and overall way for the prediction of the separation performance, while a detailed model was developed by the incorporation of non-ideal conditions. They used the 4^{th}-order Runge-Kutta method in their shooting method to iteratively solve the boundary value problem (BVP) formulation.

Khalilpour et al. [22] used the well-known Pan's model [20] and proposed a general finite difference method coupled with the Gauss-Seidel (GS) algorithm for the solution of the nonlinear membrane differential-algebraic equations. They validated their results with experimental data for natural gas sweetening. However, they did not elaborate on the details of the implementation of their numerical algorithm including convergence and computational time.

In another study, Gilassi et al. [26] proposed a numerical algorithm based on the "succession of states" in which the module is discretized into a large number of independent finite elements in which the mass-transfer driving force is constant. They iteratively used this method for the simulation of air enrichment and natural gas purification processes using single- and two-stage units of the asymmetric polymer membrane.

Lock et al. [27] utilized the finite element numerical solution for quantification of the physical aging process at different film thicknesses and operating temperatures, while using the succession of states methodology that characterizes solution diffusion model underlying membrane separation mechanism. They implemented the developed model in Aspen Hysys software for the simulation of the oxygen-enriched air combustion process.

In another work, Ebadi Amooghin et al. [28] proposed a time-dependent 2D axisymmetric model of a multilayer hollow fiber composite membrane for gas separation and validated it with experimental data. They utilized the computational fluid dynamics method on COMSOL Multiphysics with the finite element numerical approach, and concluded that temperature increase, leads to the increase of permeability and diffusion coefficient and decrease of the solubility.

Despite this rich research background, finding an efficient numerical method in terms of accuracy and speed is still an open challenge. In our previous study, a cocurrent HFM module was simulated for multicomponent gas separation by a mathematical model based on the modified shooting method [29]. Using the variable order numerical differentiation formula (NDF), the permeate outlet pressure estimation error of ~0.37% and computational time of 3.4 s were obtained.

In this work, a numerical-based algorithm was proposed to simulate the cocurrent and counter-current HFM modules for gas separation of multicomponent feed. A modified GS method with successive over-relaxation (SOR) with variable step size is utilized to obtain pressure profile, and molar flows in several membrane systems. The numerical solutions were validated by two sets of experimental data [21, 30] as well as simulated axial profiles [22].This work unifies the numerical solution algorithm for both cocurrent and counter-current modes of operation while reducing the outlet pressure estimation error to any desirable extent. It also sheds light on the details of the GS method since they are not fully covered in the open literature.

2. Modeling

The HFM is modeled as an annulus with one end closed, as shown in Figure 1. The closed end is at the same side as the feed entrance for the cocurrent mode of operation, while for the counter-current mode, the closed end is at the opposite side with respect to the feed entrance location.

The simplifying assumptions considered in this work are the ones with general acceptance in the literature:

- The gas flow is laminar and the ideal gas behavior is considered on both sides of the membrane module. In particular, it is included in the mass transfer driving force term and the derivation of the Hagen–Poiseuille equation [31].
- The permeate flows inside the fiber for which the Hagen–Poiseuille equation is used [25, 26, 27].
- The feed pressure is constant at the feed side of the membrane [27, 32].
- The effects of pressure on membrane structure and permeability are neglected. In particular, constant permeance values are assumed.
- The membrane is isothermal and thermal effects are neglected [32].
- Transient effects are neglected. Hence, the system operates at steady state [22].
- The diffusion resistance inside the pore path is negligible [25].
- The permeate fluxes of different compositions through the membrane layer have no mixing [25].

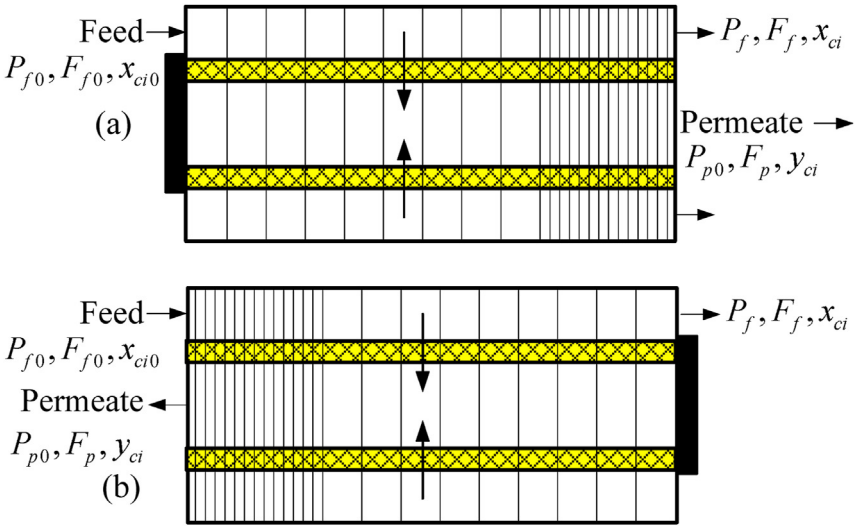

Figure 1. Schematic representation of the (a) cocurrent and (b) counter-current modes of operation with variable step size for the proposed generalized numerical framework.

The material balance for both modes of operation appears as a set of one-dimensional ordinary differential equations:

$$\frac{dF_{fi}}{dz} = -2\pi r_o N_f L K_{mi}\left(x_{ci}P_f - y_{ci}P_p\right) \tag{1}$$

where F_{fi} is the feed side flow rate of component i, r_o is the outer radius of hollow fiber, and L is its effective length. N_f, K_{mi}, x_{ci}, and y_{ci} are the number of fibers, permeance, feed-side mole fraction, and permeate-side mole fraction, respectively. The symbol z is the normalized axial coordinate. P_f is the feed-side pressure, which is considered to be constant at feed inlet pressure ($P_f = P_{f0}$). Conversely, permeate-side pressure P_p changes along the module length.

For N_c components under separation, Eq. (1) results in a set of N_c coupled nonlinear initial value differential equations. The boundary conditions for this set of differential equations in both cocurrent and counter-current modes are given at the feed flow inlet:

$$\begin{aligned} F_f(z=0) &= F_{f0} \\ x_{ci}(z=0) &= x_{ci0} \end{aligned} \tag{2}$$

noting that $F_{fi} = x_{ci}F_f$.

In Eq. (2), F_{f0} and x_{ci0} are the total feed flow rate and mole fraction of component i at the feed inlet. A set of algebraic equations is also required to complete the solution as given in Eqs. (3), (4), (5), and (6). For the cocurrent mode of operation at any point of the z-direction, for each component, the permeate flow rate for component i (F_{pi}) is obtained from the following equation:

$$F_{pi} = F_{fi0} - F_{fi} \tag{3}$$

Similarly, Eq. (4) holds for the overall mass balance in the permeate side:

$$F_p = F_{f0} - F_f \tag{4}$$

But for the counter-current mode of operation, the corresponding equations are:

$$F_{pi} = F_{fi} - F_{fi}(z=1) \tag{5}$$

$$F_p = F_f - F_f(z=1) \tag{6}$$

As mentioned in the assumptions, the pressure drop in the permeate side is obtained by the widely accepted Hagen–Poiseuille equation, which is given here for an ideal gas at temperature T flowing in a long, constant cross-section, cylindrical pipe.

$$\frac{dP_p}{dz} = \mp\frac{8RTL\mu_m F_p}{\pi r_{in}^4 N_f P_p} \tag{7}$$

where R is the universal gas constant, T is temperature, r_{in} is hollow fiber inner radius and μ_m is mixture viscosity. The minus and positive signs are for the cocurrent and counter-current modes of operation, respectively.

For the cocurrent mode of operation, the pressure is known at the outlet condition (downstream pressure, P_{p0}):

$$P_p(z=1) = P_{p0} \tag{8}$$

On the other hand, for the counter-current mode of operation, the boundary condition is defined as:

$$P_p(z=0) = P_{p0} \tag{9}$$

Eqs. (7) and (8) or (9) together form a set of ordinary differential equations. However, since the boundary conditions do not necessarily fall in a favorable position, the problem appears as a boundary value problem, which cannot be solved by the conventional numerical integration methods such as the Runge-Kutta methods. Instead, other

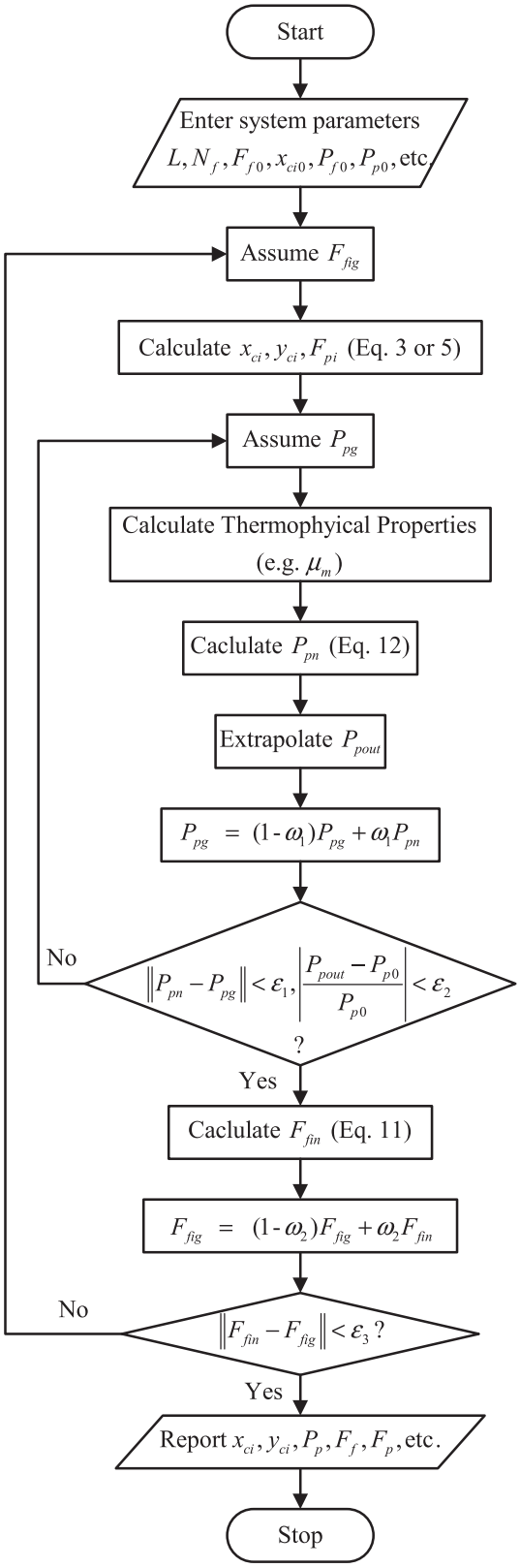

Figure 2. Flowchart of the generalized numerical solution framework.

Table 1. System parameters and operating conditions used for validation by the experimental data and simulation results.

Parameter	Unit		Value	
Temperature (T)	°C	25	25	25
Feed inlet pressure (P_{f0})	bar	4.053	21.7	30
Permeate outlet pressure (P_{pe})	bar	1.013	1.036	1.013
Length of module (L)	m	0.15	0.30	1.0
Fiber inner radius (r_{in})	μm	195	64	40
Fiber outer radius (r_o)	μm	368	160	100
Membrane area (A)	m^2	0.03	0.00905	25
Total feed flow rate (F_{f0})	mol/s	-	-	1.0
Reference	-	Tranchino et al. [30]	Choi et al. [6]	Khalilpour et al. [22]

Table 2. Feed composition and permeance values for the components used for validation.

Reference	Feed	Composition (%)	Permeance (mol/m^2sPa.)
Tranchino et al. [30]	CO_2	60	3.16×10^{-9}
	CH_4	40	8.81×10^{-10}
Choi et al. [21]	He	0.13	2.61×10^{-9}
	CH_4	67.34	6.36×10^{-11}
	CO_2	4.4	1.78×10^{-11}
	N_2	28.1	3.68×10^{-11}
Khalilpour et al. [22]	CO_2	20.0	1.34×10^{-8}
	CH_4	60.0	3.72×10^{-10}
	C_2H_6	15.0	1.02×10^{-10}
	C_3H_8	5.0	0.2×10^{-10}

methods such as the shooting method [29] or the GS iterations are required [33].

Another critical issue is the problem of stiffness, defined as the case where differential equations with significantly different rates of changes are present in the problem. In such cases, a too small integration step causes massive memory occupation and computational time, while a too large integration step results in crude accuracy [34].

Another issue that has not been thoroughly studied in the literature is the relative rate of change of variables in the axial direction. In many cases, permeate pressure takes an exponentially decaying pattern near the outlet boundary of the membrane. Similar to the stiffness issue, a too small or a too large step size for the entire solution domain is problematic. Consequently, in this work, a variable step size GS numerical framework with SOR is proposed, which can handle a wide range of problems with practical importance.

3. Numerical method

The generalized numerical framework is based on the well-known GS method with specific modifications, including SOR [33].

The SOR method is originally proposed for solving a linear system of algebraic equations derived by extrapolating the GS method. This extrapolation takes the form of a weighted average between the previous step (g) and the computed GS step (n) successively for each solution component. This approach can be readily extended to a nonlinear problem:

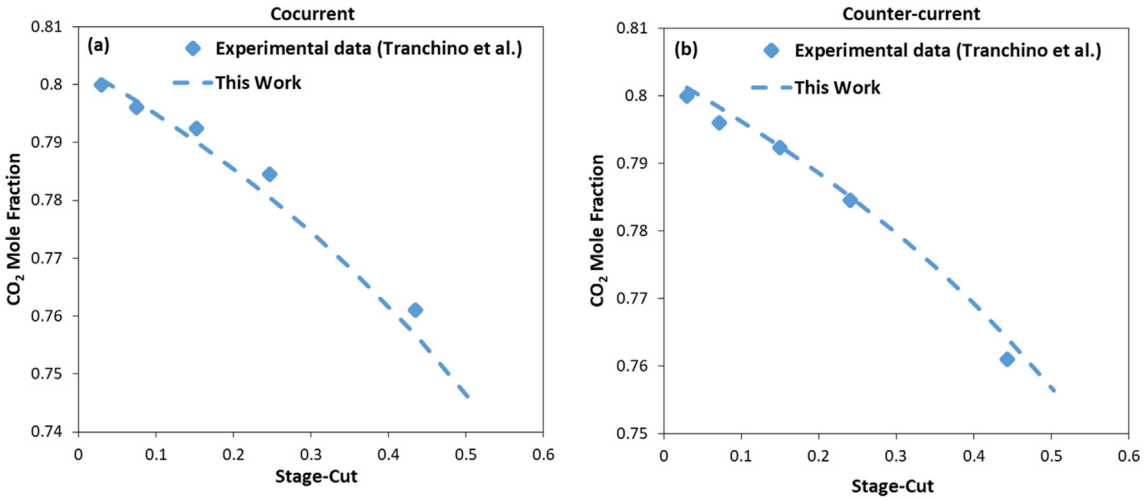

Figure 3. Comparison of the CO_2 mole fraction in the permeate side from the current work with the experimental data of Tranchino et al. [30] in the (a) cocurrent mode of operation and (b) counter-current mode of operation.

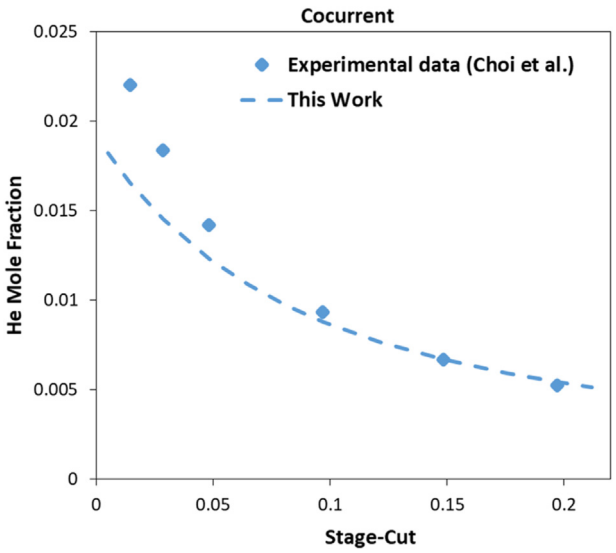

Figure 4. Comparison of the He mole fraction in the permeate side from the current work with the experimental data of Choi et al. [21].

$$x_g = (1-\omega)x_g + \omega f(x_n) \tag{10}$$

In Eq. (10), ω is the relaxation factor and f is any nonlinear function.

Using the upwind differencing scheme (UDS) [35], the discretized form of Eq. (1) transforms to the following equation:

$$F_{fin}(j) = F_{fin}(j-1) - 2\pi r_o N_f L K_{mi} \Delta z(j)\left(x_{ci}(j)P_f - y_{ci}(j)P_{pg}(j)\right) \tag{11}$$

where Δz is the step size and j is the index of the discretized point. Similarly, Eq. (7) can be converted to the following discretized form:

$$P_{pn}(j) = P_{pn}(j-1) \mp \Delta z(j)\frac{8RTL\mu_m(j)F_p(j)}{\pi r_{in}^4 N_f P_{pg}(j)} \tag{12}$$

Eqs. (11) and (12) eventually turn into a large but sparse nonlinear set of algebraic equations, which must be solved iteratively using GS method as the solution method. Moreover, the user has the option of using the most recent updates (n index) or the update from the previous iteration (g index) to calculate F_{fin} (j) and $P_{pn}(j)$.

The algorithm is given in the flowchart representation, as shown in Figure 2. It is implemented so that almost identical steps are taken for both the cocurrent and counter-current modes of operation. Moreover, the solution does not rely on using numerical integration formulas. Hence, the problem of stiffness is alleviated to a great extent in contrast to other works and even comparable to our previous study, which was solely for the cocurrent system model, which was solved by the shooting method with the variable order NDF [29].

From another point of view, as this algorithm does not rely on any commercial algebraic nor differential equation solvers, it can be readily implemented in any programming language, commercial application software or web-based applications.

The numerical algorithm comprises of two nested loops. The inner loop is responsible for the solution of the pressure equation (Eq. 12), while the outer loop is for the solution of the material balance equations (Eq. 11). While various numerical discretization schemes were tested, the simple and robust UDS with variable steps was utilized.

Using variable steps not only significantly improves the numerical accuracy, but also reduces the computational time. The variable steps take large steps in most of the solution domain, but the discretization steps are refined near the outlet zone (around $z = 1$ for the cocurrent mode and $z = 0$ for the counter-current mode of operation), which are called minor steps hereafter. This evidence emerges from the fact that pressure variation near the permeate outlet point is very sharp and nonlinear, as can be seen in the investigated case studies. It must be emphasized that the variable steps are utilized for both inner and outer loops.

Another important advantage of this numerical framework is that the solution can be started from any direction regardless of the mode of operation. For the cocurrent mode of operation, the Hagen–Poiseuille equation (Eq. 12) is discretized backward in such a way that the information from the outlet boundary condition ($z = 1$) is utilized first. However, for the counter-current mode, Eq. (12) is solved parallel to the discretized material balance equations starting from $z = 0$.

The outer loop that deals with the material balance equations is the same for both modes of operation. The only difference is calculating permeate flow, which is implemented by Eqs. (3), (4), (5), and (6).

Both loops are initialized by suitable initial guesses for pressure and molar flows in every discretization point. The initial guess for the pressure points is set at the permeate outlet pressure (P_{p0}). In the case of flow rate, a decreasing linear function of feed flow is selected as the initial guess for each component.

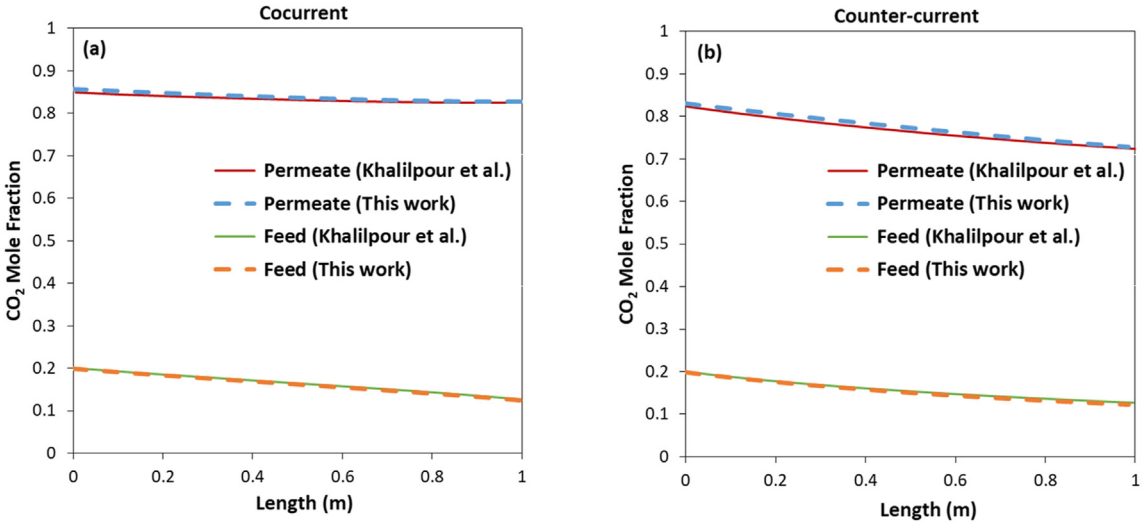

Figure 5. Comparison of the CO_2 mole fraction in the permeate and feed sides from the current work with the simulation results of Khalilpour et al. [22] in the (a) cocurrent and (b) counter-current modes of operation.

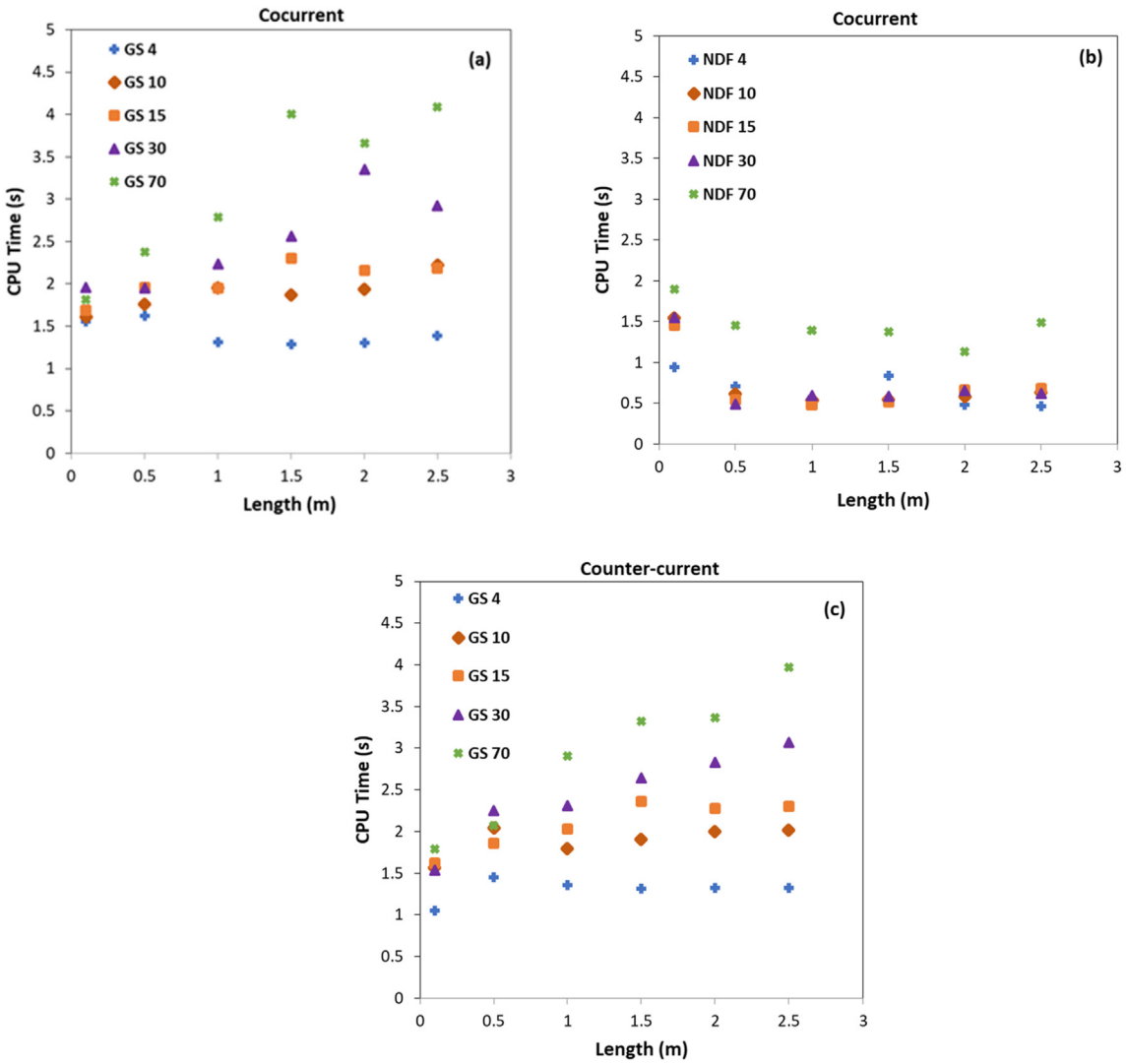

Figure 6. Computational time of (a) the GS method (cocurrent mode), (b) the shooting method of Medi and Nomvar [29] (cocurrent mode), and (c) the GS method (counter-current mode). The values in legends are feed pressure (bar).

As for the relaxation rule of the GS iterations, each time the new value is calculated, that value is modified as a weighted average of the present value and the previous value as given by Eqs. (13) and (14):

$$P_{pg} = (1-\omega_1)P_{pg} + \omega_1 P_{pn} \tag{13}$$

$$F_{fig} = (1-\omega_2)F_{fig} + \omega_2 F_{fin} \tag{14}$$

It should be noted that extrapolations are required for the counter-current mode of operation. For better accuracy, we recommend the extrapolation of feed side component molar flow (F_{fi}) to the point $z = 1$. Hence, the piecewise cubic Hermite interpolating polynomial (PCHIP) was used in this problem [36].

3.1. Convergence criteria

It is essential to elaborate on the convergence criteria of the nested loops. The inner loop (pressure loop) does not satisfy the boundary condition unless explicitly involved in the convergence criterion. Therefore, the convergence criteria for this loop are defined in two parts:

$$\left\| P_{pn} - P_{pg} \right\| < \varepsilon_1 \tag{15}$$

$$\left| \frac{P_{pout} - P_{p0}}{P_{p0}} \right| < \varepsilon_2 \tag{16}$$

Eq. (15) is the norm of the difference between current and previous estimates of pressure profiles in two consecutive iterations. It ensures that the pressure profile converges to a specific pattern. On the other hand, Eq. (16) forces the algorithm to satisfy the boundary condition where P_{pout} is the extrapolated permeate pressure at the outlet point (exactly at $z = 1$ for the cocurrent mode and $z = 0$ for the counter-current mode of operation and P_{p0} is the given permeate pressure outside the membrane module as defined earlier. ε_1 and ε_2 are small tolerances in the order of 0.01.

The outer loop that controls the flow rates only requires defining a matrix norm on the flow rates:

$$\left\| F_{fin} - F_{fig} \right\| < \varepsilon_3 \tag{17}$$

Here in Eq. (17), ε_3 is a tolerance in the order of 1×10^{-4}. The component material balance around the membrane module suggests that this approach satisfies the conservation law with reasonable accuracy.

The proposed algorithm was implemented in the MATLAB programming environment, although apart from the extrapolation tasks, no specific built-in functionality of this programming environment was utilized.

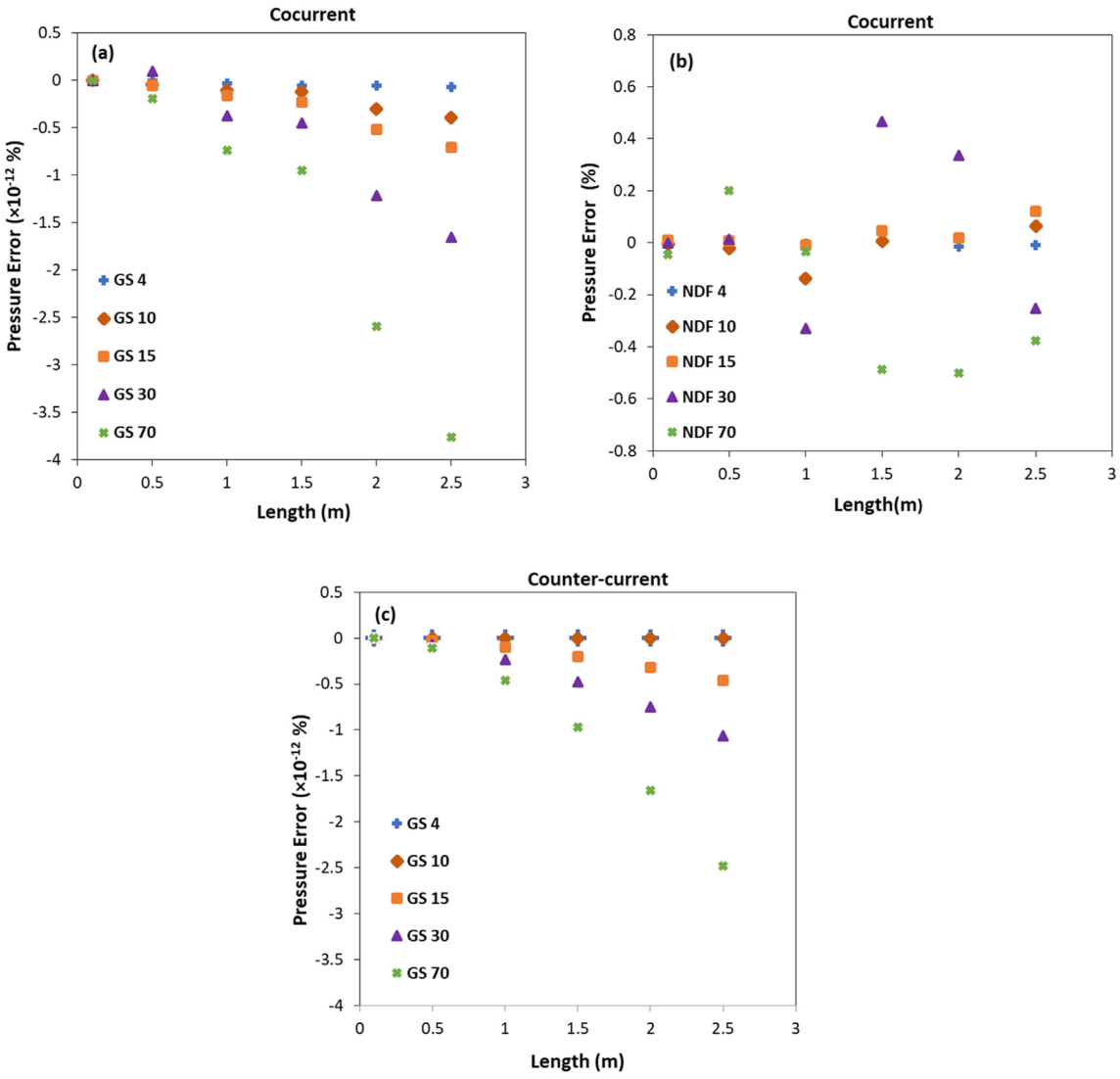

Figure 7. Permeate outlet pressure error of (a) the GS method (cocurrent mode), (b) the shooting method of Medi and Nomvar [29] (cocurrent mode), and (c) the GS method (counter-current mode). The values in legends designate feed pressure (bar).

The simulations were carried out in MATLAB 2016a on a laptop computer with an Intel Core i7-4510U (2.60 GHz) CPU with 8 GB RAM.

4. Results

4.1. Validation

In this section, the proposed numerical method is validated by comparison with the available experimental data. The first case study considers the separation of CO_2 and CH_4 in the cocurrent and counter-current modes of operation using a composite membrane [30]. The operating conditions are given in Table 1. The feed specifications and permeances are given in Table 2. The stage-cut has been changed from ca. 3–50% by varying the feed flow rate, while keeping the other operating parameters constant.

As can be seen in Figure 3, the CO_2 mole fraction decreases with increasing stage-cut. The proposed numerical method is accurate in a wide range of stage-cut values. The maximum difference is 0.4 % for both modes of operation.

The second validation case deals with the experimental separation of helium from a gas mixture of He, CO_2, N_2, and CH_4 in the cocurrent mode of operation. The separation was achieved by fabricating a highly helium-selective multilayer thin-film composite HFM for the enrichment of helium from natural gas [21]. The operating conditions are given in Table 1. The feed specifications and permeance values are given in Table 2. The validation and comparison are based on the He mole fraction in the permeate side vs. stage-cut (Figure 4). The He concentration decreases with increasing the stage-cut value in the range of ca. 1.5–20%. In this case, the accuracy is better at higher stage-cuts. However, at the lower stage-cuts, the maximum difference is about 25%. This large error can be attributed to the very small He concentration.

The numerical method is also validated by comparing axial profiles by the simulation of the CO_2 separation from a gaseous mixture in both modes of operation. The operating parameters are given in Table 1. The feed specifications and permeance values are given in Table 2, respectively. The CO_2 profile (Figure 5) shows a decreasing trend with a gentle slope along the module length. It is evident that the error is remarkably small (below 1 %) in this case.

4.2. Computational time

In the following, the proposed numerical method is assessed based on the computational time for wide ranges of membrane length (0.1–2.5 m) and feed pressure (4–70 bar). As discussed in our previous work [29],

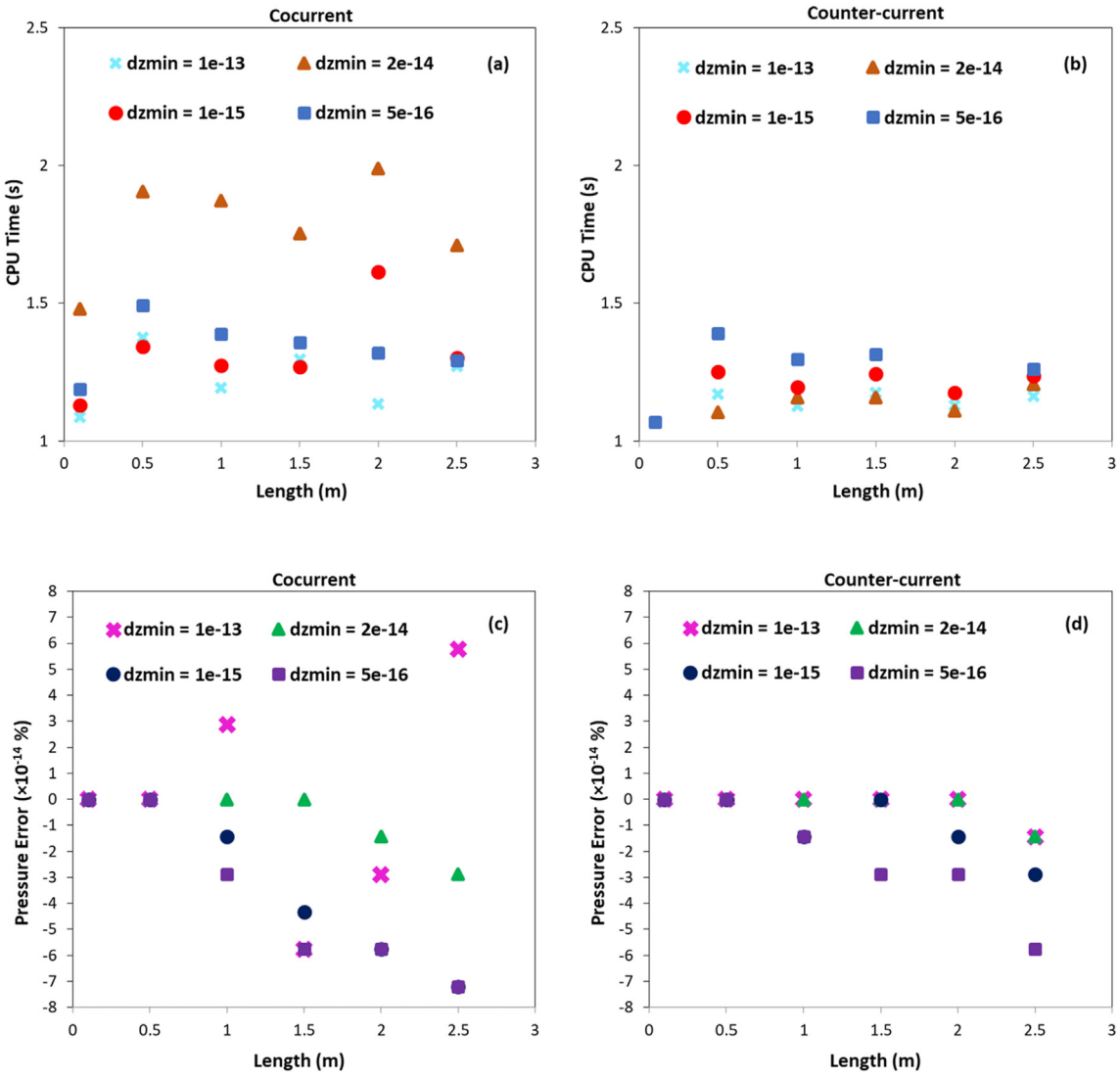

Figure 8. Computational time and permeate outlet pressure estimation error of the GS method for (a,c) the cocurrent mode and (b,d) the counter-current mode of operation for different minor step sizes. The feed pressure is fixed at 4 bar.

these ranges of operating conditions could give rise to some stiff problems, which might not be solved by the conventional variable step Runge-Kutta methods (specifically Runge-Kutta (4,5) formula, the Dormand-Prince pair [37]). Hence, the proposed numerical method is assessed on the entire ranges as given above.

In Figure 6a and c, the computational time of the proposed numerical method is given for cocurrent and counter-current modes of operation, respectively. In all cases under study, the algorithm has been successful to converge. The computational time almost monotonically increases with an increase in the membrane length and feed pressure. The maximum obtained computational time was below 4.5 s for the given ranges of membrane length and feed pressure. For the cocurrent mode, the proposed method is overall slower than the shooting method (Figure 6b) described elsewhere [29].

4.3. Accuracy

The accuracy of the present method in terms of permeate outlet pressure estimation error is calculated by Eq. (18):

$$\text{Error} = \frac{P_{p0} - P_{pout}}{P_{p0}} \times 100 \tag{18}$$

As given in Figure 7, it is apparent that the errors of the proposed numerical method (Figure 7a and c) are significantly smaller compared to the NDF method (Figure 7b), which can be mainly attributed to the variable step size approach. The minor error of the presented method can be assigned to the sensitivity of the HFM permeability toward the high-pressure side [35].

4.4. Effects of minor step size

To investigate the effects of minor step size (dz_{min}), this parameter has been changed for several representative values for the fixed feed pressure of 4 bar. The results are shown in Figure 8. As can be seen in this figure, the effects of changing minor step size are complex. In particular, the computational time does not monotonically decrease with an increase in minor step size. In the case of outlet pressure estimation error, for the counter-current mode of operation, the error almost monotonically decreases with an increase in the minor step size, which is probably due to round-off errors. For the cocurrent mode of operation, however, no such precise functionality can be derived.

In addition and for the sake of comparison, the computational time and permeate outlet pressure estimation error for a fixed step size ($dz = 0.01$ in the entire solution domain) are shown in Figure 9. For this fixed step size, the algorithm does not converge in a finite time for many

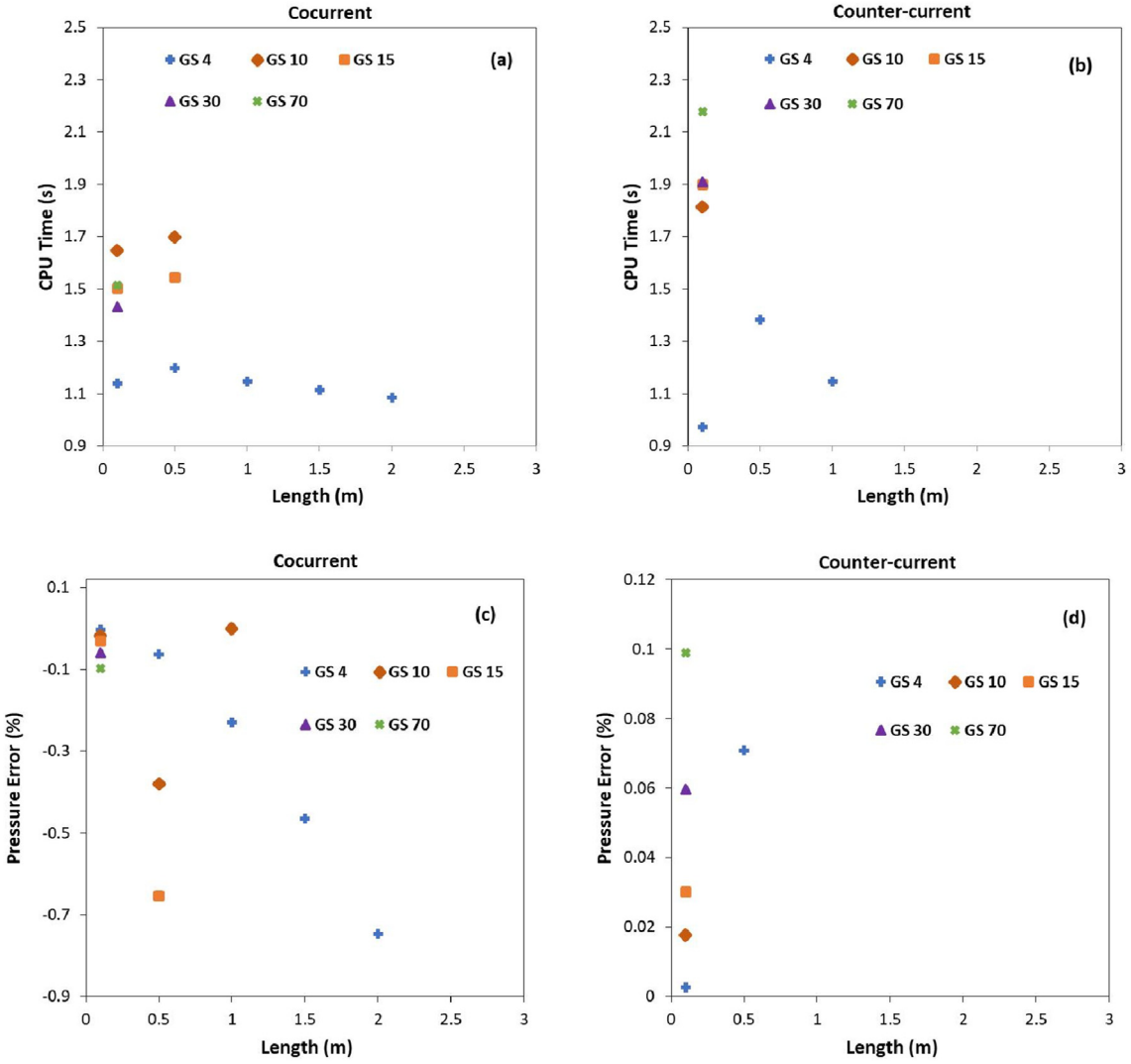

Figure 9. Computational time and permeate outlet pressure estimation error of the GS method with fixed step size ($dz = 0.01$ in the entire solution domain) for (a,c) the cocurrent mode and (b,d) the counter-current mode of operation.

operating conditions. Moreover, the permeate outlet pressure estimation error is quite large. However, it must be admitted that for many operating conditions, computational time is slightly larger for the variable step size approach though there are a few exceptions. For higher feed pressures, the variable step size approach yields a smaller computational time, which is remarkable.

5. Conclusion

The numerical solution framework based on the GS method with successive over-relaxation was successively utilized for concurrent and counter-current HFM models. In this numerical method, the variable step size results in high accuracy and low computational time. The technique has been validated by the experimental and simulation works, and good agreement was achieved.

It must be pointed that the computational time of the GS method is higher than the shooting method as implemented in our previous work. However, that shooting algorithm was only applicable for the cocurrent mode of operation and was much more complicated in the details of implementation.

The proposed numerical method is independent of differential equation solvers and can be used by any programming environment. Moreover, this method shows acceptable results in the wide ranges of module length and feed pressure. The outlet pressure estimation error of the modified GS method is as low as $\sim 10^{-14}$% with the computational time of maximum 4.5 s. Therefore, the proposed method is promising particularly for flowsheeting applications in which speed, accuracy, and reliability are all critical.

The future work can focus on the optimization of effective parameters such as feed flow rate, pressure, temperature, and membrane length. Moreover, the non-ideal behaviors such as incorporating fugacity, thermal effects, and polarization may also be considered.

Declarations

Author contribution statement

Bijan Medi: Conceived and designed the experiments; Analyzed and interpreted the data; Contributed reagents, materials, analysis tools or data; Wrote the paper.

Masoud Vesali-Naseh: Analyzed and interpreted the data; Contributed reagents, materials, analysis tools or data; Wrote the paper.

Mohaddeseh Haddad-Hamedani: Performed the experiments; Contributed reagents, materials, analysis tools or data.

Funding statement

This research did not receive any specific grant from funding agencies in the public, commercial, or not-for-profit sectors.

Data availability statement

No data was used for the research described in the article.

Declaration of interests statement

The authors declare no conflict of interest.

Additional information

No additional information is available for this paper.

References

[1] A. Shafiee, M. Nomvar, Z. Liu, A. Abbas, Automated process synthesis for optimal flowsheet design of a hybrid membrane cryogenic carbon capture process, J. Clean. Prod. 150 (2017) 309–323.
[2] Z. Dai, J. Deng, X. He, C.A. Scholes, X. Jiang, B. Wang, H. Guo, Y. Ma, L. Deng, Helium separation using membrane technology: recent advances and perspectives, Separ. Purif. Technol. 274 (2021) 119044.
[3] R. Antunes, O. Borisevich, D. Demange, Numerical analysis of H2/He gas separation experiments performed with a MFI-type tubular zeolite membrane, Chem. Eng. Res. Des. 109 (2016) 327–334.
[4] D.Y. Kim, S. Ryu, H.-J. Kim, H.C. Ham, H. Sohn, S.P. Yoon, J. Han, T.-H. Lim, J.Y. Kim, S.W. Lee, C.W. Yoon, S.H. Choi, Highly selective asymmetric polybenzimidazole-4,4′-(hexafluoroisopropylidene) bis(benzoic acid) hollow fiber membranes for hydrogen separation, Separ. Purif. Technol. 257 (2021) 117954.
[5] S.P. Kaldis, G.C. Kapantaidakis, G.P. Sakellaropoulos, Simulation of multicomponent gas separation in a hollow fiber membrane by orthogonal collocation — hydrogen recovery from refinery gases, J. Membr. Sci. 173 (2000) 61–71.
[6] S.-H. Choi, M.S. Qahtani, E.A. Qasem, Multilayer thin-film composite membranes for helium enrichment, J. Membr. Sci. 553 (2018) 180–188.
[7] M. Vesali-Naseh, M.R. Vesali Naseh, P. Ameri, Adsorption of Pb (II) ions from aqueous solutions using carbon nanotubes: a systematic review, J. Clean. Prod. 291 (2021) 125917.
[8] Y. Xu, Y. Yu, Y. Yang, T. Sun, S. Dong, H. Yang, Y. Liu, X. Fan, C. Song, Improved separation performance of carbon nanotube hollow fiber membrane by peroxydisulfate activation, Separ. Purif. Technol. 276 (2021) 119328.
[9] A. Behboudi, Y. Jafarzadeh, R. Yegani, Incorporation of silica grafted silver nanoparticles into polyvinyl chloride/polycarbonate hollow fiber membranes for pharmaceutical wastewater treatment, Chem. Eng. Res. Des. 135 (2018) 153–165.
[10] R. Schopf, F. Schmidt, U. Kulozik, Impact of hollow fiber membrane length on the milk protein fractionation, J. Membr. Sci. 620 (2021) 118834.
[11] N. Alikhani, D.W. Bousfield, J. Wang, L. Li, M. Tajvidi, Numerical simulation of the water vapor separation of a moisture-selective hollow-fiber membrane for the application in wood drying processes, Membranes 11 (2021).
[12] J.-L. Li, B.-H. Chen, Review of CO2 absorption using chemical solvents in hollow fiber membrane contactors, Separ. Purif. Technol. 41 (2005) 109–122.
[13] D. Aaron, C. Tsouris, Separation of CO_2 from flue gas: a review, Separ. Sci. Technol. 40 (2005) 321–348.
[14] Y. Chu, A. Lindbråthen, L. Lei, X. He, M. Hillestad, Mathematical modeling and process parametric study of CO_2 removal from natural gas by hollow fiber membranes, Chem. Eng. Res. Des. 148 (2019) 45–55.
[15] T. Katoh, M. Tokumura, H. Yoshikawa, Y. Kawase, Dynamic simulation of multicomponent gas separation by hollow-fiber membrane module: nonideal mixing flows in permeate and residue sides using the tanks-in-series model, Separ. Purif. Technol. 76 (2011) 362–372.
[16] S. Sharifian, M. Harasek, B. Haddadi, Simulation of membrane gas separation process using aspen Plus® V8.6, Chem. Prod. Process Model. 11 (2016) 67.
[17] J. Marriott, E. Sørensen, A general approach to modelling membrane modules, Chem. Eng. Sci. 58 (2003) 4975–4990.
[18] J.A. Dehkordi, S.S. Hosseini, P.K. Kundu, N.R. Tan, Mathematical modeling of natural gas separation using hollow fiber membrane modules by application of finite element method through statistical analysis, Chem. Prod. Process Model. 11 (2016) 11–15.
[19] G. Dibrov, M. Ivanov, M. Semyashkin, V. Sudin, G. Kagramanov, High-pressure aging of asymmetric Torlon® hollow fibers for helium separation from natural gas, Fibers 6 (2018).
[20] C.Y. Pan, Gas separation by high-flux, asymmetric hollow-fiber membrane, AIChE J. 32 (1986) 2020–2027.
[21] S.-H. Choi, M.M.B. Sultan, A.A. Alsuwailem, S.M. Zuabi, Preparation and characterization of multilayer thin-film composite hollow fiber membranes for helium extraction from its mixtures, Separ. Purif. Technol. 222 (2019) 152–161.
[22] R. Khalilpour, A. Abbas, Z. Lai, I. Pinnau, Analysis of hollow fibre membrane systems for multicomponent gas separation, Chem. Eng. Res. Des. 91 (2013) 332–347.
[23] E. Pardyjak, Boundary Value Problems, Chapter 27, 2018. Available from: http://www.mech.utah.edu/∼pardyjak/me6700/Lect15_BoundEigenvalueProblemsCh27.pdf.
[24] A.S. Kovvali, S. Vemury, W. Admassu, Modeling of multicomponent countercurrent gas permeators, Ind. Eng. Chem. Res. 33 (1994) 896–903.
[25] S.S. Hosseini, S.M. Roodashti, P.K. Kundu, N.R. Tan, Transport properties of asymmetric hollow fiber membrane permeators for practical applications: mathematical modelling for binary gas mixtures, Can. J. Chem. Eng. 93 (2015) 1275–1287.
[26] S. Gilassi, S.M. Taghavi, D. Rodrigue, S. Kaliaguine, Simulation of gas separation using partial element stage cut modeling of hollow fiber membrane modules, AIChE J. 64 (2018) 1766–1777.
[27] S.S.M. Lock, K.K. Lau, A.M. Shariff, Y.F. Yeong, Z.H. Ban, W.H. Tay, Process simulation and optimization of oxygen enriched combustion using thin polymeric membranes: effect of thickness and temperature dependent physical aging, J. Chem. Technol. Biotechnol. 94 (2019) 2844–2868.
[28] A. Ebadi Amooghin, S. Mirrezaei, H. Sanaeepur, M.M. Moftakhari Sharifzadeh, Gas permeation modeling through a multilayer hollow fiber composite membrane, J. Membr. Sci. Res. 6 (2020) 125–134.
[29] B. Medi, M. Nomvar, Developing a fast and robust numerical method for the simulation of cocurrent hollow fiber gas separation membranes for process flowsheet synthesis, SN Appl. Sci. 2 (2020) 426.
[30] L. Tranchino, R. Santarossa, F. Carta, C. Fabiani, L. Bimbi, Gas separation in a membrane unit: experimental results and theoretical predictions, Separ. Sci. Technol. 24 (1989) 1207–1226.
[31] A.S. Berman, Laminar flow in channels with porous walls, J. Appl. Phys. 24 (1953) 1232–1235.
[32] X. Feng, J. Ivory, V.S.V. Rajan, Air separation by integrally asymmetric hollow-fiber membranes, AIChE J. 45 (1999) 2142–2152.
[33] A. Hadjidimos, Successive over relaxation (SOR) and related methods, J. Comput. Appl. Math. 123 (2000) 177–199.
[34] J.R. Cash, Modified extended backward differentiation formulae for the numerical solution of stiff initial value problems in ODEs and DAEs, J. Comput. Appl. Math. 125 (2000) 117–130.
[35] B. Medi, M. Amanullah, Application of a finite-volume method in the simulation of chromatographic systems: effects of flux limiters, Ind. Eng. Chem. Res. 50 (2011) 1739–1748.
[36] C.B. Moler, Numerical Computing with MATLAB: Revised Reprint, Society for Industrial and Applied Mathematics (SIAM), Philadelphia, PA, 2008.
[37] J.R. Dormand, P.J. Prince, A family of embedded Runge-Kutta formulae, J. Comput. Appl. Math. 6 (1980) 19–26.